

Experience-Dependent Plasticity in Accessory Olfactory Bulb Interneurons following Male–Male Social Interaction

 Hillary L. Cansler,^{1,2} Marina A. Maksimova,¹ and  Julian P. Meeks¹

¹Department of Neuroscience, and ²Neuroscience Graduate Program, Graduate Program of Biomedical Sciences, The University of Texas Southwestern Medical Center, Dallas, Texas 75390

Chemosensory information processing in the mouse accessory olfactory system guides the expression of social behavior. After salient chemosensory encounters, the accessory olfactory bulb (AOB) experiences changes in the balance of excitation and inhibition at reciprocal synapses between mitral cells (MCs) and local interneurons. The mechanisms underlying these changes remain controversial. Moreover, it remains unclear whether MC–interneuron plasticity is unique to specific behaviors, such as mating, or whether it is a more general feature of the AOB circuit. Here, we describe targeted electrophysiological studies of AOB inhibitory internal granule cells (IGCs), many of which upregulate the immediate-early gene *Arc* after male–male social experience. Following the resident–intruder paradigm, *Arc*-expressing IGCs in acute AOB slices from resident males displayed stronger excitation than nonexpressing neighbors when sensory inputs were stimulated. The increased excitability of *Arc*-expressing IGCs was not correlated with changes in the strength or number of excitatory synapses with MCs but was instead associated with increased intrinsic excitability and decreased HCN channel-mediated I_H currents. Consistent with increased inhibition by IGCs, MCs responded to sensory input stimulation with decreased depolarization and spiking following resident–intruder encounters. These results reveal that nonmating behaviors drive AOB inhibitory plasticity and indicate that increased MC inhibition involves intrinsic excitability changes in *Arc*-expressing interneurons.

Key words: accessory olfactory bulb; chemical senses; experience-dependent plasticity; interneuron; intrinsic excitability; sensory processing

Significance Statement

The accessory olfactory bulb (AOB) is a site of experience-dependent plasticity between excitatory mitral cells (MCs) and inhibitory internal granule cells (IGCs), but the physiological mechanisms and behavioral conditions driving this plasticity remain unclear. Here, we report studies of AOB neuronal plasticity following male–male social chemosensory encounters. We show that the plasticity-associated immediate-early gene *Arc* is selectively expressed in IGCs from resident males following the resident–intruder assay. After behavior, *Arc*-expressing IGCs are more strongly excited by sensory input stimulation and MC activation is suppressed. *Arc*-expressing IGCs do not show increased excitatory synaptic drive but instead show increased intrinsic excitability. These data indicate that MC–IGC plasticity is induced after male–male social chemosensory encounters, resulting in enhanced MC suppression by *Arc*-expressing IGCs.

Introduction

A central goal in neuroscience is to understand how sensory processing in the brain guides behavior. The mammalian accessory

olfactory system (AOS) is an attractive neural pathway for studying the processes linking sensation and behavior because the AOS has a relatively linear circuit pathway into the brain and drives a variety of social behaviors (for review, see Liberles, 2014). In the AOS, sensory information is generated in the vomeronasal organ (VNO) and is processed by a single dedicated neural circuit, the accessory olfactory bulb (AOB), before being sent to limbic struc-

Received April 17, 2017; revised June 1, 2017; accepted June 22, 2017.

Author contributions: H.L.C. and J.P.M. designed research; H.L.C. and M.A.M. performed research; J.P.M. contributed unpublished reagents/analytic tools; H.L.C. and J.P.M. analyzed data; H.L.C. and J.P.M. wrote the paper.

This work was funded by the National Institute on Deafness and Other Communication Disorders and the National Institute on Drug Abuse of the National Institutes of Health under award numbers R00-DC-011780 and R01-DC-015784 (to J.P.M.), and T32-DA-007290 (to H.L.C.). Partial support was also provided by the National Science Foundation (Grant IOS-1451034; to J.P.M., co-Principal Investigator). The content is solely the responsibility of the authors and does not necessarily represent the official views of the National Institutes of Health. We thank Jennifer Torres, Salma Ferdous, and Natasha Browder for technical support. We also thank Kimberly Huber and Todd Roberts for critical feedback on the manuscript.

The authors declare no competing financial interests.

Correspondence should be addressed to Julian P. Meeks, 5323 Harry Hines Boulevard, MC 9111, NB4.204D, Dallas, TX 75390. E-mail: julian.meeks@utsouthwestern.edu.

DOI:10.1523/JNEUROSCI.1031-17.2017

Copyright © 2017 the authors 0270-6474/17/377240-13\$15.00/0

tures, including the medial amygdala and bed nucleus of the stria terminalis (Scalia and Winans, 1975). Animals lacking proper AOS signaling display a range of atypical behaviors, including deficits in predator avoidance (Papes et al., 2010; Pérez-Gómez et al., 2015), courtship (Pankevich et al., 2004; Kimchi et al., 2007; Ferrero et al., 2013), and territorial aggression (Stowers et al., 2002; Chamero et al., 2007; Leinders-Zuffall et al., 2014). Though many of these behaviors are considered innate, behavioral and physiological evidence suggests that the AOB is a site of experience-dependent plasticity. This has been best studied in the context of pregnancy block, in which a female forms a chemosensory memory of her recent mate but remains unexplored in the context of other AOS-mediated social behaviors (Bruce, 1959; Brennan et al., 1990).

There is still much to learn about how the AOB contributes to plasticity in social behaviors. In pregnancy block, one hypothesis proposes that inhibitory gain limits the activation of AOB projection neurons, called mitral cells (MCs) to the chemosensory cues of a recent mate (for review, see Brennan, 2009). Increased inhibition involves changes at reciprocal dendrodendritic synapses between MCs and AOB interneurons (Brennan et al., 1990; Araneda and Firestein, 2006; Larriva-Sahd, 2008; Brennan, 2009; Smith et al., 2009). It remains unclear whether such inhibition is induced by other social chemosensory encounters, and the specific neuronal populations that contribute to these effects are not yet clear.

Immediate early genes (IEGs) are expressed in recently active neurons and can provide extensive information about the cells and networks that participate in sensory and behavioral experiences (Kawashima et al., 2013; Kim et al., 2015; Vousden et al., 2015). The IEG *Arc* is both an important plasticity-related gene and a useful marker of neuronal populations engaged by experience (for review, see Shepherd and Bear, 2011). *Arc* is typically expressed in principal excitatory neurons (cortical and hippocampal pyramidal neurons), where it mediates many forms of experience-dependent synaptic plasticity (Plath et al., 2006; Vazdarjanova et al., 2006; Jakkamsetti et al., 2013). Studies of *Arc* expression in the AOB show that it is selectively upregulated in subsets of AOB internal granule cells (IGCs), but not MCs, in male and female rodents after mating (Matsuoka et al., 2002a, 2003). *Arc* expression by interneurons has also been noted in the main olfactory bulb in several studies (Guthrie et al., 2000; Vazdarjanova et al., 2006; Shakhawat et al., 2014). The selective expression of *Arc* by interneurons is atypical, and studying these populations is likely to provide new insights into the role of *Arc* in nonprincipal neuronal types.

Here, we report that *Arc* is selectively expressed in posterior AOB (pAOB) IGCs of male mice following the resident–intruder territorial aggression assay. *Arc* upregulation by IGCs required intact vomeronasal signaling, indicating that centrifugal inputs were not sufficient to induce *Arc* in this behavioral paradigm. Following resident–intruder behavior, *Arc*-expressing IGCs in resident males showed enhanced network excitation compared with nonexpressing IGCs, while MC activity was suppressed. We investigated the IGC physiological features that underlie their enhanced activity and found no evidence for an increase in excitatory synapse strength or number. Instead, we found that *Arc*-expressing IGCs display a robust increase in intrinsic excitability compared with other IGCs. Our results show that AOB inhibitory plasticity occurs after nonmating behaviors and reveal cellular mechanisms underlying MC inhibition after chemosensory social encounters.

Materials and Methods

Mice. All animal procedures were in compliance with the University of Texas Southwestern Institutional Care and Use Committee. Sexually naive adult male mice aged 6–12 weeks were housed on a customized 12 h

light/dark cycle with the lights on from noon until midnight. Food and water were provided *ad libitum*. *Arc-d4EGFP-BAC* (a gift from Pavel Osten Cold Spring Harbor Laboratory, Cold Spring Harbor, NY; Grinevich et al., 2009) and *Arc^{tm1St}* (*Arc*^{-/-} or *Arc*-d2EGFP; stock #007662, The Jackson Laboratory; RRID:IMSR_JAX:007662; Wang et al., 2006) mice were generous gifts from Kimberly Huber (UT Southwestern Medical Center, Dallas, TX). *Trpc2^{tm1Dlc}* (*Trpc2*^{-/-}; stock #021208, The Jackson Laboratory; RRID:IMSR_JAX:021208; Stowers et al., 2002), and *Gt(ROSA)26Sor^{tm9(CAG-tdTomato)Hze}* (*Ai9*; stock #007905, The Jackson Laboratory; RRID:IMSR_JAX:007905; Madisen et al., 2010) mice were obtained from The Jackson Laboratory. A total of 119 mice were used in this study.

Experimental design. Resident male mice were individually housed on corn cob bedding, without cage changes, for 1 week before the experiment. All behavior occurred during the dark phase [zeitgeber time 20 (ZT20) to ZT24] in a dimly lit room to facilitate video recording. After a 10 min habituation period, a BALB/cJ male intruder mouse was introduced to the resident cage for a 10 min encounter. To test the response to soiled bedding alone, a small Petri dish was filled with bedding from a cage of four BALB/cJ males that had gone without cage changes for 1 week. This Petri dish was introduced into the resident's cage for 10 min instead of an intruder animal. Following behavior, imaging and electrophysiological experiments were performed as described below in detail.

Live slice preparation. Animals were anesthetized with isoflurane and decapitated 3 h after the resident–intruder paradigm was completed, unless otherwise specified. Brains were dissected, and 400 μ m parasagittal sections of the AOB were prepared using a Leica VT1200 vibrating microtome in ice-cold, oxygenated artificial CSF (ACSF). The ACSF contained 125 mM NaCl, 2.5 mM KCl, 2 mM CaCl₂, 1 mM MgCl₂, 25 mM NaHCO₃, 1.25 mM NaH₂PO₄, 25 mM glucose, 3 mM myo-inositol, 2 mM Na-pyruvate, and 0.4 mM Na-ascorbate, with an additional 9 mM MgCl₂ in the slicing buffer. After slicing, the slices were kept in a recovery chamber at room temperature (22°C) containing ACSF with 0.5 mM kynurenic acid to prevent potential glutamate excitotoxicity during the recovery/holding period. Just before recordings, slices were transferred to a slice chamber (Warner Instruments) mounted on a fluorescence and differential interference contrast imaging-equipped upright microscope (Model FN1, Nikon). Oxygenated ACSF was superfused via a peristaltic pump (Gilson) at a rate of 1–2 ml/min throughout. Slice temperature was maintained at 32–33°C via in-line and chamber heaters (Warner Instruments).

Two-photon imaging and image analysis. Image stacks up to 200 μ m deep were acquired using an excitation wavelength of 890 nm and a 40 \times [1.0 numerical aperture (NA)] water-immersion objective (Olympus). Images were denoised using a 3D median filter and deconvolved using a model point spread function in ImageJ (RRID:SCR_003070). Fluorescent cells were counted using a 3D object-counting add-on (Bolte and Cordelières, 2006). Cell counts were normalized to the volume of the cell layer of interest. $I_{Arc\text{sum}}$ was computed as follows:

$$I_{Arc\text{sum}} = \frac{\sum_{i=1}^n I_{Arc(i)}}{x \mu m^3},$$

where $I_{Arc(i)}$ is the normalized brightness of each cell ($I_{Arc(i)} = \frac{B_i}{K}$). B_i is the mean pixel intensity within cellular region of interest I , K is the mean pixel intensity within the internal cellular layer (ICL) but outside cellular regions of interest, and x is the total volume within the imaged portion of the ICL. This metric combines the relative brightness of all identified cells and is normalized by the imaged volume to facilitate comparisons across experimental preparations.

Immunohistochemistry. Following behavior, animals were briefly anesthetized with inhaled isoflurane, then injected with a ketamine/xylazine cocktail (120 mg/kg ketamine/16 mg/kg xylazine dose) and transcardially perfused with 0.01 M PBS followed by 4% paraformaldehyde (PFA) in PBS. Brains were postfixed in 4% PFA in PBS overnight. Brains were then cryoprotected overnight in PBS containing 25% sucrose, embedded in OCT compound (TissueTek), and flash frozen. The 30 μ m sections were prepared using a Leica CM3050 S cryostat and were processed free floating. Sections were rinsed four times in 0.01 M PBS, incubated in 0.1%

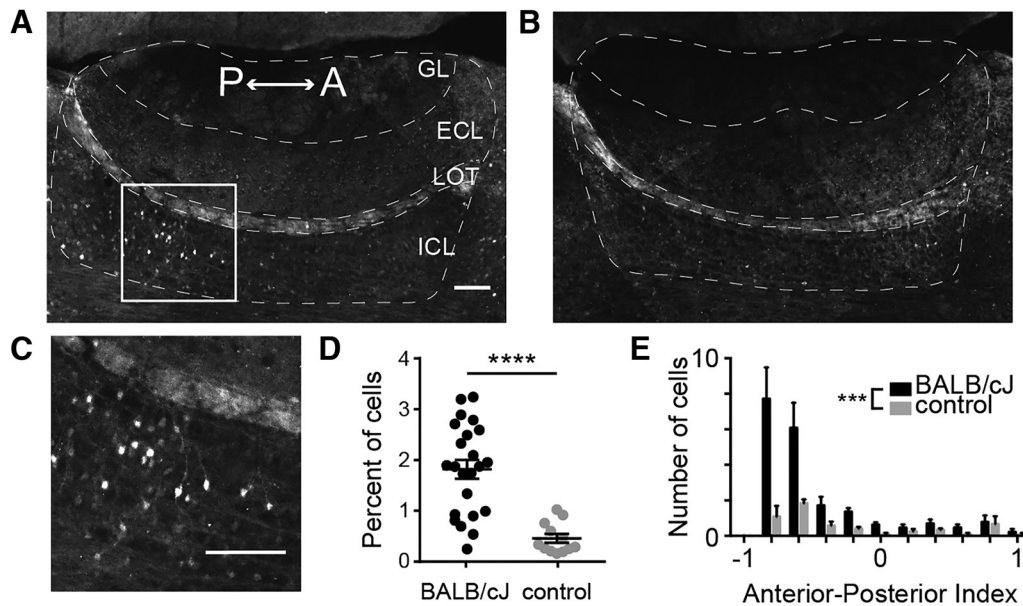


Figure 1. Exposing resident males to novel male intruders results in upregulation Arc protein expression in AOB IGCs. **A**, Parasagittal section through the AOB of a C57BL/6J male resident 90 min after being exposed to a BALB/cJ male intruder. Immunofluorescence indicates Arc protein expression. Scale bar, 100 μ m. $n = 6$ animals, 23 sections. GL, Glomerular layer; LOT, lateral olfactory tract. **B**, AOB section from a control resident that was not exposed to an intruder. $n = 3$ animals, 12 sections. **C**, Enhanced view of IGCs in the boxed area in **A**. **D**, Percentage of all cells expressing somatic Arc protein. Wilcoxon–Mann–Whitney test, **** $p < 0.0001$. Scale bar, 100 μ m. **E**, Normalized anterior–posterior position of Arc-expressing cells in the ICL. Wilcoxon–Mann–Whitney test, *** $p < 0.001$.

Triton X-100 in PBS for 2 h, rinsed three times, incubated in 10% goat serum in PBS for 2 h, and incubated in primary antibody in primary block (0.1% Triton X-100, 10% goat serum in PBS) overnight at 4°C. Sections were then rinsed three times in PBS and incubated in secondary antibody in secondary block (0.1% Triton X-100, 5% goat serum) for 2 h. Sections were rinsed three times, incubated in 500 nM DAPI in PBS, and rinsed three additional times. Sections were then mounted on slides in Fluoromount-G Mounting Medium (SouthernBiotech). Anti-Arc primary antibody specificity (rabbit polyclonal antibody; catalog #156003, Synaptic Systems; RRID:AB_887694) was verified using *Arc*^{-/-} mice and was used at 1:1000. Anti-GFP primary (chicken polyclonal antibody; catalog #ab13970, Abcam; RRID:AB_300798) was used at 1:500. Goat anti-rabbit AF633 (catalog #A21070, Invitrogen; RRID:AB_2535731) and goat anti-chicken AF488 (catalog #A11039, Invitrogen; RRID:AB_142924) were both used at 1:2000 dilution.

Biocytin amplification of filled neurons was achieved using streptavidin-Alexa Fluor 568 (catalog #S11226, Thermo Fisher; RRID:AB_2315774). Slices were washed in PBS three times for 30 min each. Slices were then incubated in a blocking solution containing 0.5% Triton X-100 and 10% goat serum in PBS for 2 h, followed by the same blocking solution containing streptavidin-AF568 at 0.01 mg/ml for 4 h. Slices were then rinsed three times for 30 min each and mounted on slides in Fluoromount-G Mounting Medium.

For the experiments seen in Figures 2 and 5, immunostained sections were imaged with a 40 \times (1.3 NA) oil-immersion objective on an LSM 510 Inverted Confocal Microscope (Zeiss). For the experiments in Figure 1, immunostained sections were imaged with a Zeiss Axioscan.Z1 microscope using a 20 \times (0.8 NA) air-objective. Cells were counted manually using ImageJ by a scorer blinded to the experimental condition. The anterior–posterior index was calculated using custom MATLAB software. Spines were counted, and morphological analysis performed using the Simple Neuron Tracer plugin for ImageJ (Longair et al., 2011) by a scorer blinded to experimental conditions. Spines were counted on the 100 μ m of primary dendrite in the external cellular layer (ECL) starting at the edge of the lateral olfactory tract.

Electrophysiology. Whole-cell patch-clamp recordings were made on destabilized EGFP with a 4 h half-life-positive (d4EGFP⁺) and d4EGFP⁻ IGCs during a window spanning 4–8 h following behavior. Thin wall borosilicate glass electrodes with a tip resistance between 4 and 12 M Ω were filled with internal solution containing the following (in mM): 115 K-gluconate, 20

KCl, 10 HEPES, 2 EGTA, 2 MgATP, 0.3 Na₂GTP, 10 Na phosphocreatine at pH 7.37. All recordings were amplified using a MultiClamp 700B amplifier (Molecular Devices) at 20 kHz and were digitized by a DigiData 1440 analog-digital converter controlled via pClamp 10.5 software (Molecular Devices; RRID:SCR_011323). Data were analyzed by Clampex 10.5 (Molecular Devices) and custom software written in MATLAB.

For glomerular stimulation experiments, a theta glass-stimulating electrode was placed in the glomerular layer while recordings were made from IGCs. A series of 0.3 ms single pulses was used to construct input–output curves (Stimulus Isolator A365RC, World Precision Instruments), and the stimulation intensity for 20 Hz trains was the highest subsaturating value from the input–output analysis. One d4EGFP⁺ and one d4EGFP⁻ neuron were recorded per slice (one at a time). The d4EGFP⁺ neuron was recorded first in 6 of 10 pairs. Input–output curves were generated for each neuron, but the stimulation intensity used for both was chosen based on the first neuron recorded. Before MC recordings, we confirmed that stimulus conditions effectively recruited IGCs through direct IGC patch-clamp recordings (23 of 24 recordings).

For miniature EPSC (mEPSC) recordings, 5 min of baseline activity was recorded, then 1 μ M TTX was washed on for 5 min, and 5 min of postdrug activity was recorded. Biocytin (3 mg/ml) and/or Alexa Fluor 568 (166 μ M) was added to the internal solution to visualize dendritic arbors and spines. After filling, slices were fixed in 4% PFA in PBS for 1 h and then stored in PBS at 4°C.

To assess intrinsic electrophysiological features, we subjected patched AOB neurons to a series of current-clamp and voltage-clamp challenges. Immediately after achieving the whole-cell configuration, the resting membrane potential (V_{rest}) of each cell was measured in current-clamp mode. To standardize measurements across cells with different V_{rest} s we injected steady-state currents to maintain the membrane potential (V_m) of each cell between -70 and -75 mV. Based on initial measurements of input resistance (R_{input}), we empirically determined the amplitude of hyperpolarizing current that adjusted V_m by -50 mV (to approximately -125 mV). After determining this initial current injection amplitude, we generated a cell-specific 10-sweep Clampex protocol that applied increasingly depolarizing 0.5 s square current pulses, starting with the initial injection amplitude. For example, if the initial current injection was determined to be -100 pA, the 10-sweep protocol would have current injection increments of $+20$ pA (i.e., $-100, -80, -60, \dots +80$ pA). If the initial depolarization was determined to be -125 pA, the protocol

Table 1. Parameters used for multidimensional analysis

Shorthand	Description	Mode	Method	Reference
V_{rest}	Resting membrane potential	I Clamp	Direct measurement	N/A
C_m	Membrane capacitance			
R_m	Input resistance			
N_{comps}	Number of model compartments	I Clamp	See reference	Golowasch et al., 2009
$I_{h,sag}$	Hyperpolarization-induced depolarizing potential	I Clamp	$I_{h,sag} = V_{init} - V_{ss}$	N/A
$I_{h,current}$	Hyperpolarization-induced depolarizing current	V Clamp	$I_{h,curr} = I_{init} - I_{ss}$	N/A
EPSC_freq	Mean spontaneous EPSC frequency	V Clamp		
EPSC_amp	Mean spontaneous EPSC amplitude	V Clamp	Direct measurement after waveform sorting	Hendrickson et al., 2008
EPSC_tau	Mean spontaneous EPSC decay constant	V Clamp	Least-squares exponential decay	N/A
S_{freq_1}	Spiking frequency: Lv. 1	I Clamp	Direct measurement	N/A
S_{freq_2}	Spiking frequency: Lv. 2	I Clamp	Direct measurement	N/A
S_{freq_3}	Spiking frequency: Lv. 3	I Clamp	Direct measurement	N/A
S_{freq_4}	Spiking frequency: Lv. 4	I Clamp	Direct measurement	N/A
$S1_{slope}$	Initial action potential rising slope	I Clamp	Initial spike derivative peak	
$S1_{thresh}$	Initial action potential threshold	I Clamp	V_m at 10% of initial spike derivative	Meeks et al., 2005
S_{accom_1}	Spike rate accommodation: Lv. 1	I Clamp		
S_{accom_2}	Spike rate accommodation: Lv. 2	I Clamp		
S_{accom_3}	Spike rate accommodation: Lv. 3	I Clamp		
S_{accom_4}	Spike rate accommodation: Lv. 4	I Clamp	$\frac{S_{init} - S_{final}}{S_{init} + S_{final}}$	N/A
Na_{curr_1}	Voltage-gated sodium current amplitude: Lv. 1	V Clamp	Direct measurement	N/A
Na_{curr_2}	Voltage-gated sodium current amplitude: Lv. 2	V Clamp	Direct measurement	N/A
Na_{curr_3}	Voltage-gated sodium current amplitude: Lv. 3	V Clamp	Direct measurement	N/A
Na_{curr_4}	Voltage-gated sodium current amplitude: Lv. 4	V Clamp	Direct measurement	N/A
Na_{curr_5}	Voltage-gated sodium current amplitude: Lv. 5	V Clamp	Direct measurement	N/A
K_{curr_max}	Voltage-gated potassium current: maximum	V Clamp	Direct measurement	N/A
K_{curr_diff}	Noninactivating voltage-gated potassium current	V Clamp	Direct measurement	N/A

N/A, Not applicable; Lv., level; V Clamp, voltage clamp; I Clamp, current clamp.

would include increments of, for example, +25 pA. This strategy allowed us to objectively challenge cells with widely varying V_{rest} and R_{input} values. In voltage clamp, cells were initially held at -70 mV, and a series of 12 voltage command steps (0.5 s in duration) were applied that spanned -100 to $+10$ mV.

For each cell, both current-clamp and voltage-clamp protocols were applied up to four times, and all reported quantities represent the mean responses across repeated trials. Twenty-six specific intrinsic parameters were extracted from each cell using custom software written in MATLAB. A description of the parameters seen in Figure 6A and the formulas used to calculate them is presented in Table 1. The hyperpolarization-activated cation (I_H) current ratio (see Fig. 6G) was calculated using the following formula:

$$\frac{I_{init} - I_{ss}}{I_{init}}$$

where I_{init} is the mean initial current (measured between 10 and 160 ms following the voltage pulse) and I_{ss} is the mean steady-state current (measured between 420 and 470 ms after the voltage pulse) generated by a voltage command step from -70 to -100 mV. EPSCs were automatically detected and later separated from noise using a custom computer-assisted waveform-based event-sorting program written in MATLAB (Hendrickson et al., 2008). EPSC decay was measured by calculating the best fit exponentially decaying line for the decay period of the EPSC. Initial action potential rising slope was calculated by measuring the peak of the first derivative of voltage with respect to time (dV/dt). Threshold was defined as V_m at the time the dV/dt voltage reached 10% of its peak value (similar to Meeks et al., 2005). Membrane capacitance and input resistance were calculated according to current clamp-based multicompartamental algorithms (Golowasch et al., 2009). Briefly, the voltage response of each cell to a hyperpolarizing current step was fit with a series of multiexponential curves, and the best fit was determined by identifying the solution with the lowest value of the Bayesian Information Criterion (to avoid overfitting).

Statistical Analysis. Unless otherwise indicated, comparisons between two groups were made using the nonparametric Wilcoxon–Mann–Whitney test. Comparisons involving multiple experimental groups were made using one-way ANOVA. Repeated-measures ANOVA was used for

20 Hz glomerular stimulation experiments. Statistical significance threshold was set at $p < 0.05$ for all comparisons.

Results

Arc expression is upregulated in posterior AOB IGCs following resident–intruder encounters

Arc is expressed in IGCs in rodents shortly after mating, an AOS-mediated behavior that induces pheromonal memory formation in females (Bruce and Parrott, 1960; Brennan et al., 1995; Mat-suoka et al., 2002a, 2003). If experience-dependent plasticity in the AOB is a more general response to chemosensory social events, we hypothesized that the social chemosensory encounters associated with male–male territorial aggression, which is AOS mediated, would induce AOB plasticity. We used the resident–intruder paradigm, which is known to encourage AOS-dependent territorial aggression between males, as our behavioral challenge (Maruniak et al., 1986; Stowers et al., 2002). Adult male wild-type C57BL/6J residents were housed individually for 1 week and then exposed to adult male BALB/cJ intruders for 10 min. Arc protein expression was significantly increased 90 min after the behavior in AOB IGCs of resident males compared with controls (Wilcoxon–Mann–Whitney test, $p < 0.0001$; Fig. 1A–D). Previous studies indicated that male–male resident–intruder encounters increase Fos expression in the pAOB, which is selectively innervated by vomeronasal sensory neurons (VSNs) that express members of the V2R subfamily of vomeronasal receptors (Belluscio et al., 1999; Kumar et al., 1999; Rodriguez et al., 1999; Chamero et al., 2007). Consistent with these results, Arc protein expression after the resident–intruder paradigm was selectively upregulated in pAOB IGCs (Wilcoxon–Mann–Whitney test, $p < 0.001$; Fig. 1E). These initial results show that Arc expression in IGCs following resident–intruder behavior is similar to Arc expression following mating behavior and suggest that Arc expression oc-

curs in an interneuron population that might increase MC inhibition after resident–intruder encounters.

Arc-d4EGFP-BAC tools mark *Arc*-expressing IGCs in a time- and chemosignal-dependent manner

To identify *Arc*-expressing IGCs in live tissue, we used *Arc-d4EGFP-BAC* reporter mice (Grinevich et al., 2009). In these mice, d4EGFP is expressed under the control of the *Arc* promoter on a bacterial artificial chromosome, leaving endogenous *Arc* unperturbed. To assess the *Arc-d4EGFP-BAC* reporter, we used *Arc-d4EGFP-BAC* male mice as residents in the resident–intruder paradigm. We sacrificed animals at various time points following behavior (Fig. 2A) and compared *Arc* protein and d4EGFP immunostaining levels to controls (no intruder, BALB/cj male soiled bedding only; Fig. 2A–D). *Arc* protein expression began rising by 30 min postbehavior, peaked 1–2 h postbehavior and returned to baseline by 4 h postbehavior (one-way ANOVA, $F_{(7,11)} = 18.64$, $p < 0.0001$; $n = 1$ –2 mice and 2–3 sections/condition; 11 mice and 19 sections overall; Fig. 2A,C). d4EGFP levels increased significantly by 1 h postbehavior and remained elevated at 4 h postbehavior (one-way ANOVA, $F_{(7,11)} = 13.07$, $p = 0.0002$; Fig. 2A,D). We observed strong colocalization between the *Arc* protein and d4EGFP signals, while some cells showed d4EGFP signal but no *Arc* protein in the cell soma. This effect could be explained by the fact that *Arc* protein is often localized to the dendrites (Shepherd and Bear, 2011) and that low levels of d4EGFP expression (indicating low-level *Arc* transcription) were boosted by immunostaining.

Because d4EGFP immunostaining boosts very weak signals, we wanted to test whether d4EGFP expression alone was sufficient to identify *Arc*-expressing cells in living tissue. Live two-photon imaging of acute AOB slices from *Arc-d4EGFP-BAC* residents revealed robust d4EGFP expression starting at 3 h postbehavior and remaining strong until 6 h postbehavior (Fig. 2E). Thus, unamplified d4EGFP signals lag behind the immunostaining time course, which is likely due to differences in antibody-amplified versus native d4EGFP signals. Importantly, the time window including the strongest behaviorally driven d4EGFP expression was well aligned with the time course of acute slice electrophysiological experiments, making the *Arc-d4EGFP-BAC* mice a strong tool for investigating the physiological properties of *Arc*-expressing IGCs.

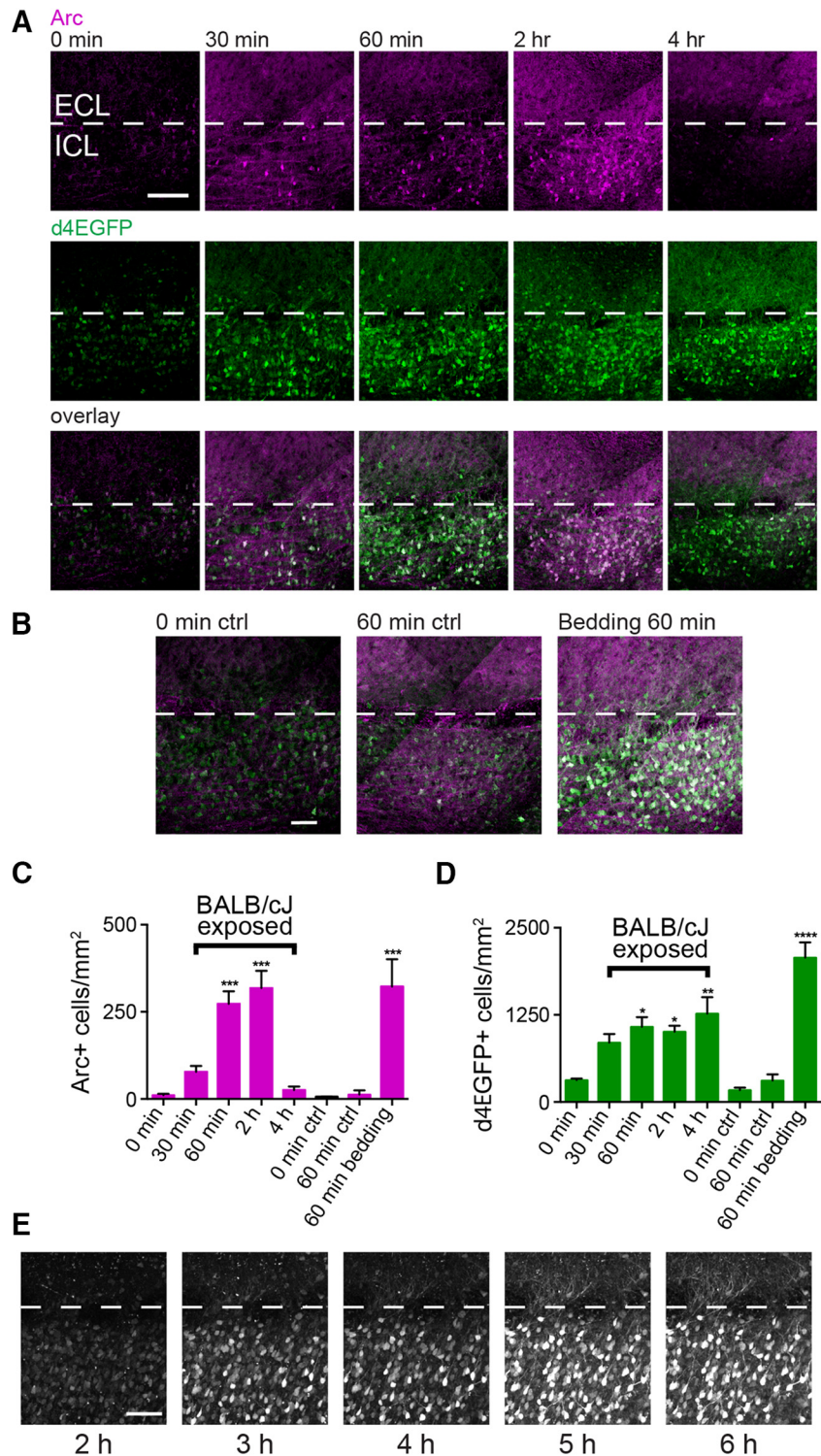


Figure 2. *Arc* protein expression peaks 2 h after behavior and overlaps with d4EGFP expression in *Arc-d4EGFP-BAC* mice. **A**, Parasagittal AOB sections from resident mice perfused 0, 30, 60, 120, or 240 min after behavior, stained for both *Arc* protein and d4EGFP. The ICL is indicated by white dotted lines, and posterior AOB is shown. Scale bar, 100 μ m. **B**, *Arc* protein and d4EGFP expression in negative control mice that were perfused after 0 or 60 min in the behavioral setup but were not exposed to a BALB/cj intruder (left two panels). *Arc* protein and d4EGFP expression in a resident mouse that was exposed to soiled BALB/cj bedding only in the behavioral setup then was perfused 60 min later. Scale bar, 50 μ m. **C**, Quantification of *Arc* immunostaining across conditions. One-way ANOVA, $F_{(7,11)} = 18.64$, $p < 0.0001$. **D**, Quantification of d4EGFP immunostaining across conditions. One-way ANOVA, $F_{(7,11)} = 13.07$, $p = 0.0002$. For **C** and **D**: * $p < 0.05$, ** $p < 0.01$, *** $p < 0.001$, and **** $p < 0.0001$, compared with the 0 min controls (19 sections across 11 mice; ANOVA corrected for multiple comparisons using Dunnett's method). **E**, Time course of d4EGFP expression in a single acute live slice visualized using two-photon microscopy. Each image is a maximum z-projection of a 200 μ m slice. Dissection occurred 1 h after behavior. Scale bar, 100 μ m. ctrl, Control.

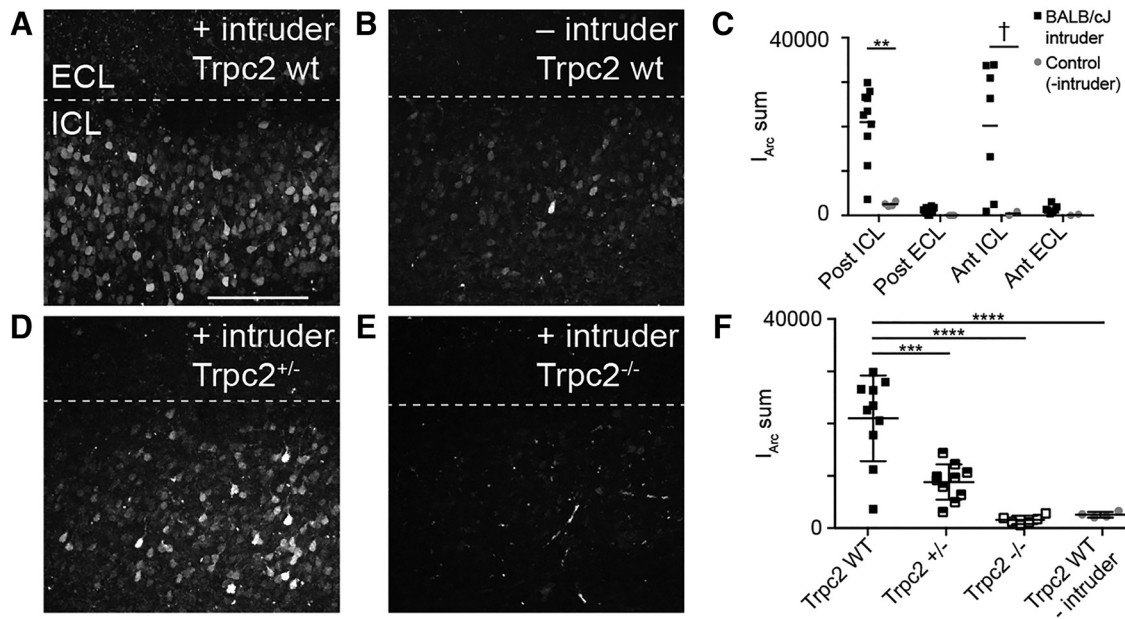


Figure 3. *Arc* expression is not upregulated after the resident–intruder assay in *Trpc2*^{-/-} mice. **A**, Maximum z-projection of an acute AOB slice taken from an *Arc-d4EGFP-BAC*, *Trpc2*^{+/+} resident. Posterior AOB is shown. Images were taken 4 h after exposure to a BALB/cJ intruder. Scale bar, 200 μ m. **B**, Representative z-projection taken from a control resident that was not exposed to an intruder. **C**, Quantification of summed fluorescence intensity across d4EGFP-expressing cells (*I*_{Arc} sum). Significance in each region was determined using the Wilcoxon–Mann–Whitney test: ***p* < 0.01; †*p* < 0.1. Posterior ICL: *n* = 9 mice, 10 slices (experimental), *n* = 4 mice, 4 slices (control); posterior ECL: *n* = 9 mice, 10 slices (experimental), *n* = 3 mice, 3 slices (control); anterior ICL/ECL: *n* = 6 mice, 7 slices (experimental) *n* = 2 mice, 2 slices (control). **D**, Representative z-projection taken from a *Trpc2*^{+/-} *Arc-d4EGFP-BAC* male resident. **E**, Representative z-projection taken from a *Trpc2*^{-/-} *Arc-d4EGFP-BAC* male resident. **F**, Quantification of *I*_{Arc} sum for the posterior ICL of all genotypes. *Trpc2*^{+/+}, *n* = 5 mice, 10 slices; *Trpc2*^{-/-}, *n* = 3 mice, 6 slices. One-way ANOVA, $F_{(3,26)} = 22.75$, *p* < 0.0001. ****p* < 0.001, *****p* < 0.0001 for indicated pairs (corrected for multiple comparisons using Tukey’s method).

Before we tested *Arc*-expressing IGC physiology, we wanted to determine whether d4EGFP expression required AOS sensory activation. This was important because different salient behaviors can activate centrifugal input into the entire olfactory bulb (Shipley et al., 1985; Brennan et al., 1990; Nunez-Parra et al., 2013; Rothermel et al., 2014; Oetl et al., 2016). Previous studies of AOB IEG expression indicated that chemosensory stimulation alone (soiled bedding) is sufficient to induce *Arc* expression and that social interaction increases this effect (Matsuoka et al., 2002b). Having confirmed that AOS chemosensory stimulation alone was sufficient to induce robust *Arc* expression (Fig. 2B–D), we wanted to next determine whether AOS activation was necessary for *Arc* expression. To accomplish this, we backcrossed *Arc-d4EGFP-BAC* reporter mice into a *Trpc2*^{-/-} background. *Trpc2*, which is expressed in all vomeronasal sensory neurons and a small percentage of main olfactory sensory neurons, is required for proper chemosensory transduction (Omura and Mombaerts, 2014). Thus, *Trpc2*^{-/-} mice have severely disrupted vomeronasal chemosensory transduction and profound changes to AOS-mediated behaviors while retaining most main olfactory function (Stowers et al., 2002; Kimchi et al., 2007; Papes et al., 2010). We introduced *Arc-d4EGFP-BAC*, *Trpc2*^{-/-} resident males to BALB/cJ male intruders and imaged acutely prepared live AOB slices using two-photon microscopy 4 h postbehavior, a time of robust d4EGFP expression after resident–intruder behaviors (Fig. 3). We quantified d4EGFP expression in the posterior ICL for *Trpc2*^{+/+}, *Trpc2*^{+/-}, and *Trpc2*^{-/-} animals exposed to intruders, as well as *Trpc2*^{+/+} residents that were left alone in an empty cage (no intruder) for 10 min (Fig. 3A–F). Compared with the *Trpc2* wild-type mice, all other groups showed significantly reduced d4EGFP expression (one-way ANOVA: $F_{(3,26)} = 22.75$, *p* < 0.0001; Fig. 3F). This reduction occurred despite the fact that *Trpc2*^{-/-} animals do not display deficits in olfactory social investi-

gation (Stowers et al., 2002). Total d4EGFP intensity in *Trpc2*^{-/-} animals exposed to intruders matched that of *Trpc2*^{+/+} animals left alone in an empty cage, indicating that sensory input from VSNs is necessary for the elevated *Arc* expression in AOB IGCs (Fig. 3F). These results show that *Arc-d4EGFP-BAC* reporter mice label *Arc*-expressing IGCs in living AOB tissue and also show that VSN activation is both necessary and sufficient to induce AOB *Arc* expression after resident–intruder encounters.

Arc-expressing IGCs respond strongly to glomerular stimulation

Previous work showed experience-dependent increases in inhibitory tone in the AOB following salient social behavior, suggesting that IGCs increase their inhibitory influence on MC output (Brennan et al., 1990, 1995). If the IGCs expressing *Arc* after social chemosensory interactions contribute to AOB experience-dependent plasticity, we hypothesized that *Arc*-expressing IGCs would respond differently to AOB sensory input than nonexpressing IGCs. To test this hypothesis, we made targeted whole-cell patch-clamp recordings from *Arc*-expressing (d4EGFP⁺) and nonexpressing (d4EGFP⁻) IGCs in acute slices 4–8 h after resident–intruder experiments (Fig. 4). To simulate sensory activity, we electrically stimulated VSN fibers in the AOB glomerular layer using theta-glass electrodes. Stimulating the glomerular layer induces glutamate release from VSN terminals and activates downstream MCs, which in turn activate IGCs at dendrodendritic synapses (Fig. 4A). Thus, IGC activation resulting from VSN terminal stimulation is a disinaptic effect. In voltage clamp, *Arc*-expressing IGCs showed increased single-pulse EPSC charge transfer and peak current amplitude compared with nonexpressing IGCs across stimulus intensities (paired, two-tailed Student’s *t* test, *p* < 0.05; *n* = 10 slices across seven mice; Fig. 4B–F). d4EGFP⁺ IGCs were recorded first in 6 of 10 experiments, so we

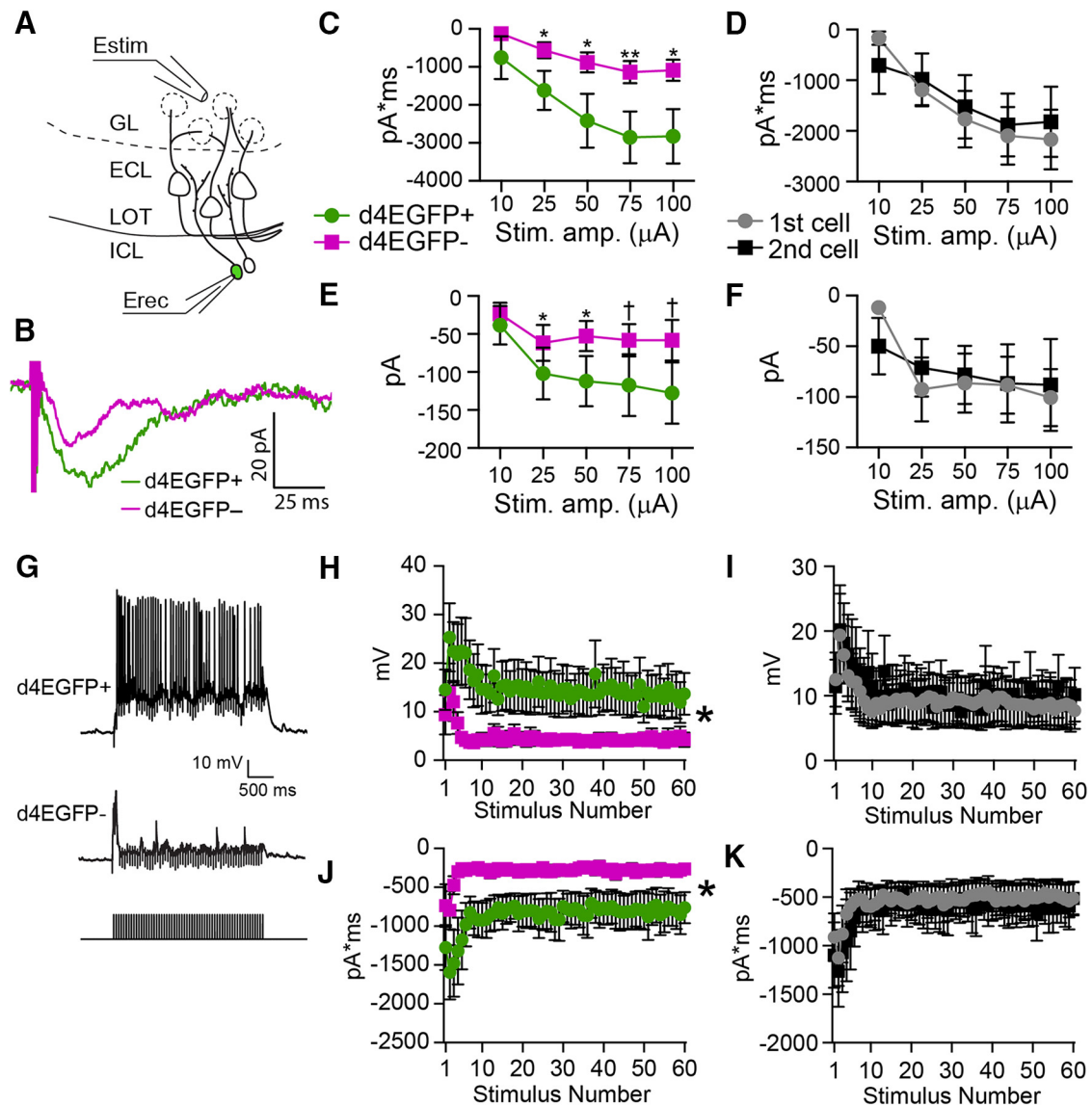


Figure 4. *Arc*-expressing IGCs show increased excitation by glomerular layer stimulation. **A**, Diagram illustrating experimental setup. Estim, Theta glass stimulating electrode; Erec, recording electrode. **B**, Sample responses from a single, equal amplitude electrical stimulus from a d4EGFP⁺ cell and a nearby d4EGFP⁻ cell from the same slice. **C**, Input–output curves showing charge transfer in response to a single stimulus pulse for d4EGFP⁺ and d4EGFP⁻ cells. Paired, two-tailed Student's *t* test: * $p < 0.05$, ** $p < 0.01$. **D**, Same data as from **C**, grouped by the order in which the cells were recorded rather than d4EGFP expression. **E**, Input–output curves showing EPSC amplitude in response to a single pulse; data grouped by d4EGFP expression. Paired, two-tailed Student's *t* test: † $p < 0.1$; * $p < 0.05$. **F**, Same data from **E**, grouped by the order in which cells were recorded. **G**, Sample traces from d4EGFP⁺ and d4EGFP⁻ IGCs responding to 3 s, 20 Hz stimulation. **H**, Peak amplitude reached in response to each pulse of a 3 s, 20 Hz stimulus train. Repeated-measures ANOVA, main effect of group: $F_{(1,18)} = 4.51$, $p = 0.048$. **I**, Same data from **H**, grouped by the recording order. Repeated-measures ANOVA, no main effect of group: $F_{(1,18)} = 0.03$, $p = 0.87$. **J**, Total charge transfer in response to each pulse of the 3 s, 20 Hz stimulus train. Repeated-measures ANOVA, main effect of group: $F_{(1,18)} = 5.52$, $p = 0.03$. **K**, Same data from **J**, grouped by recording order. Repeated-measures ANOVA, no main effect of group: $F_{(1,18)} = 0.07$, $p = 0.79$. For all panels, $n = 7$ mice, 10 slices, 10 pairs. Stim. amp., Stimulus amplitude.

investigated possible order effects by comparing these same responses based on the recording order (Fig. 4*D,F*). We found no differences in this comparison (paired, two-tailed Student's *t* test, $p > 0.05$), indicating that order effects cannot explain the increased excitability of d4EGFP⁺ IGCs. To evaluate the physiological relevance of these responses, we approximated strong MC activation by delivering a 3 s, 20 Hz train of stimuli to glomerular layer (matching MC firing rates measured during direct chemosensory stimulation of the VNO; Meeks et al., 2010). In current clamp, d4EGFP⁺ IGCs responded to trains with increased peak amplitudes, which were also sustained throughout the 3 s stimulus (repeated-measures ANOVA, main effect of group: $F_{(1,18)} = 4.51$, $p = 0.048$; Fig. 4*G,H*). This effect was eliminated when the same data were organized based on recording order (repeated-

measures ANOVA, no main effect of group: $F_{(1,18)} = 0.03$, $p = 0.87$; Fig. 4*I*). In voltage clamp, the same d4EGFP⁺ IGCs responded to stimulus trains with significantly greater charge transfer than d4EGFP⁻ IGCs and sustained this increase throughout the 3 s of stimulation (repeated-measures ANOVA, main effect of group: $F_{(1,18)} = 5.52$, $p = 0.03$; Fig. 4*J*). As before, this effect was not due to an effect of recording order (repeated-measures ANOVA, no main effect of group: $F_{(1,18)} = 0.07$, $p = 0.79$; Fig. 4*K*). These data indicate that *Arc*-expressing IGCs are more engaged by sensory input stimulation, which may reflect enhanced MC–IGC synaptic communication or increased IGC intrinsic excitability. These data also suggest that *Arc*-expressing IGCs may contribute to experience-dependent MC inhibition.

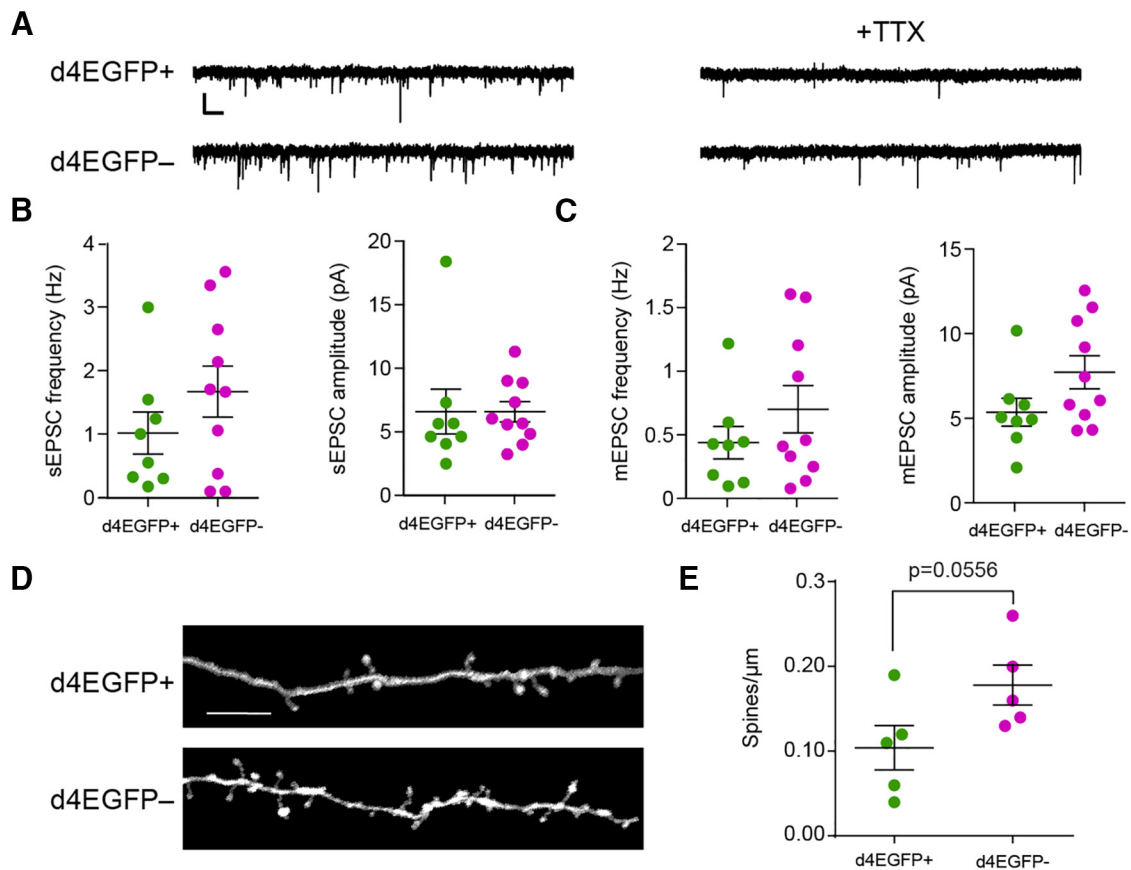


Figure 5. *Arc*-expressing IGCs do not display enhanced synaptic strength or number compared with nonexpressing IGCs. **A**, Sample sEPSC and mEPSC traces from d4EGFP⁺ and d4EGFP⁻ neurons. Calibration: 10 pA, 500 ms. **B**, Spontaneous frequency and amplitude in d4EGFP⁺ IGCs. Significance determined using Wilcoxon–Mann–Whitney test (n.s., $p > 0.05$). d4EGFP⁺, $n = 8$; d4EGFP⁻, $n = 10$; n mice = 10. **C**, Mini-frequency and amplitude of d4EGFP⁺ and d4EGFP⁻ IGCs. Significance determined using Wilcoxon–Mann–Whitney test (n.s., $p > 0.05$). d4EGFP⁺, $n = 8$; d4EGFP⁻, $n = 10$; n = 10 mice. **D**, Representative images showing dendritic spines on d4EGFP⁺ and d4EGFP⁻ IGCs. Scale bar, 10 μ m. **E**, Spines per micrometer for d4EGFP⁺ and d4EGFP⁻ neurons. Significance determined using Wilcoxon–Mann–Whitney test. d4EGFP⁺ cells, $n = 5$; d4EGFP⁻ cells, $n = 5$; n = 5 mice.

Arc-expressing IGCs do not possess increased synapse strength or density

We hypothesized that the increased activation of *Arc*-expressing IGCs was due to a change in the number of MC–IGC synapses or a change in MC–IGC synaptic strength. To test these hypotheses, we recorded spontaneous EPSCs (sEPSCs) and mEPSCs from d4EGFP⁺ and d4EGFP⁻ IGCs (Fig. 5). *Arc*-expressing IGCs did not exhibit a significant difference in sEPSC or mEPSC amplitude or frequency (Wilcoxon–Mann–Whitney test, $p > 0.05$; Fig. 5A–C). In these experiments, biocytin was included in the recording pipette to allow *post hoc* analysis of dendrite morphology and dendritic spine density. Analysis of IGC dendrites showed a trend toward slightly lower spine densities in *Arc*-expressing IGCs compared with nonexpressing IGCs (Wilcoxon–Mann–Whitney test, $p = 0.0556$; Fig. 5D,E). Similarly, there were no differences in average dendritic branch length (d4EGFP⁺: $485.3 \pm 115.7 \mu$ m, $n = 6$; d4EGFP⁻: $365.5 \pm 57.2 \mu$ m, $n = 8$; Wilcoxon–Mann–Whitney test, $p = 0.57$), maximum dendritic branch length (d4EGFP⁺: $1813 \pm 149.4 \mu$ m, $n = 6$; d4EGFP⁻: $1548 \pm 231.4 \mu$ m, $n = 8$; Wilcoxon–Mann–Whitney test, $p = 0.41$), or the number of branches (d4EGFP⁺: 17.5 ± 4.75 branches, $n = 6$; d4EGFP⁻: 14.3 ± 1.89 branches, $n = 8$; Wilcoxon–Mann–Whitney test, $p = 0.59$). Together, these results indicate that changes in IGC synaptic strength or number cannot explain the increased responses to glomerular stimulation in *Arc*-expressing IGCs.

Arc-expressing IGCs possess enhanced intrinsic excitability

Lacking support for our initial hypothesis, we turned to an alternative, which was that *Arc*-expressing IGCs respond more strongly to VSN input stimulation due to changes in intrinsic properties. We used a systematic approach to assess possible intrinsic physiological differences in an unbiased way. We targeted whole-cell patch-clamp recordings to *Arc*-expressing and nonexpressing IGCs 4–8 h postbehavior and delivered a series of electrophysiological challenges in current and voltage clamp. Using automated algorithms (see Experimental procedures), we quantified 26 physiological characteristics covering a variety of intrinsic properties (Table 1). To capture the differences between *Arc*-expressing and nonexpressing IGCs, we performed cluster analysis on the 26-dimensional array of characteristics from 100 neurons that had undergone the same electrophysiological challenges (Fig. 6A,B). This collection of cells contained 26 d4EGFP⁺ and 23 d4EGFP⁻ cells, along with 39 control IGCs from mice that had not undergone behavioral challenges and 12 MCs (used as a control population; Fig. 6A,B). Four clusters were identified by this analysis. A total of 69.2% of all d4EGFP⁺ IGCs were assigned to cluster 3, where neurons exhibited sustained strong spiking activity in response to depolarization and lower levels of spike accommodation. Other intrinsic characteristics, including input resistance, resting membrane potential, and action potential threshold, were highly variable across cells in

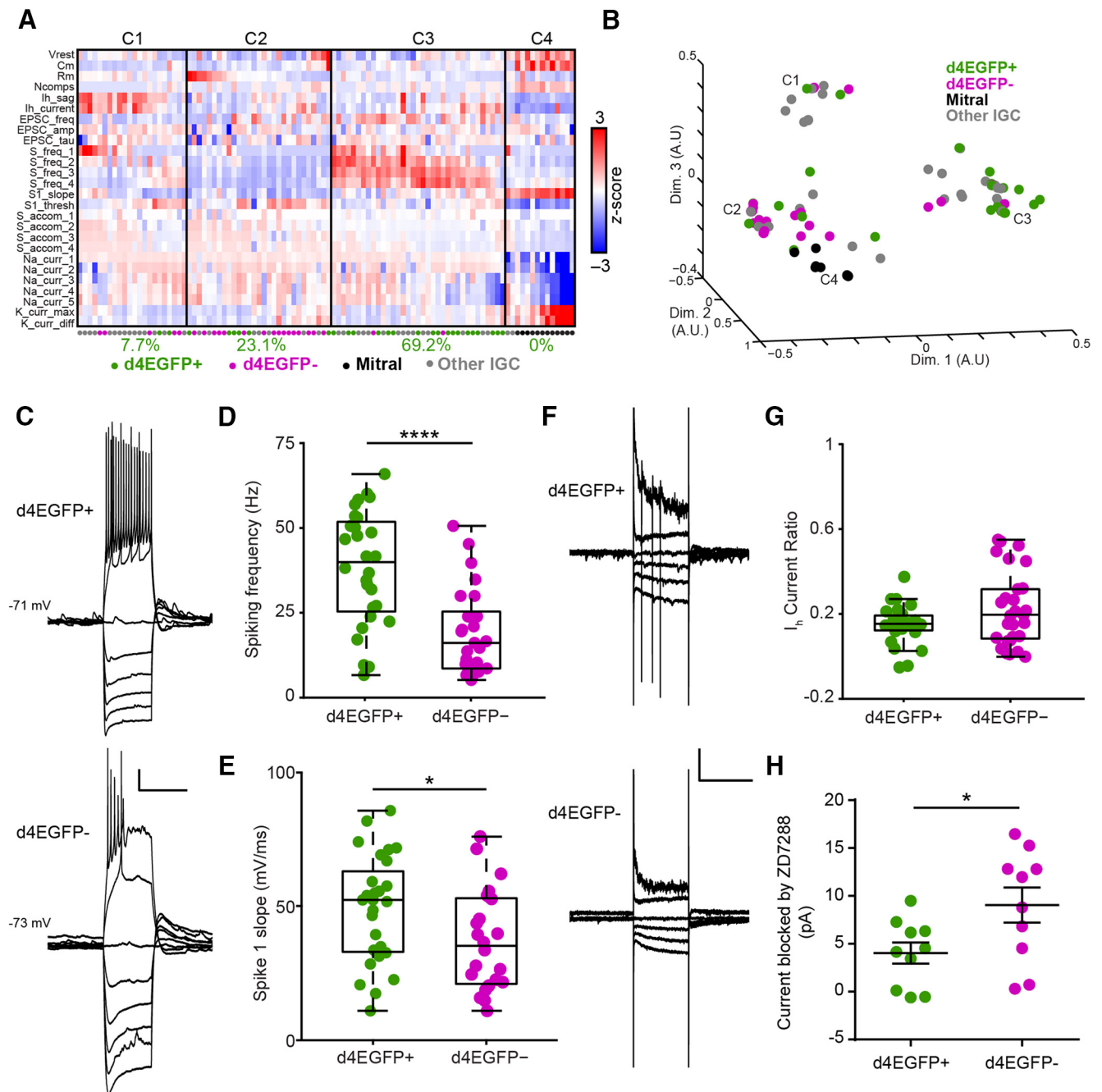


Figure 6. *Arc*-expressing IGCs are intrinsically more excitable than nonexpressing IGCs. **A**, Colorized heat map representation of 26 intrinsic descriptors (rows) across 100 AOB neurons (columns) that were subjected to current-clamp and voltage-clamp challenges. Solid vertical lines indicate divisions between identified clusters. Below each cluster is the percentage of all d4EGFP⁺ IGCs within that cluster. **B**, Multidimensional scaling of relative differences across all 26 dimensions from **A** into three dimensions. Each individual colored point indicates a cell, and C1–C4 refer to the cluster definitions in **A**. For **A** and **B**: d4EGFP⁺ IGCs, $n = 26$; d4EGFP⁻ IGCs, $n = 23$; $n = 15$ animals; other IGCs, $n = 39$; mitral, $n = 12$; $n = 37$ animals. **C**, Sample traces for d4EGFP⁺ and d4EGFP⁻ IGCs for current-clamp ramp challenges. Calibration: 10 mV, 500 ms. **D**, d4EGFP⁺ IGCs exhibit significantly increased spiking frequency when depolarized by a current injection (d4EGFP⁺, $n = 26$; d4EGFP⁻, $n = 23$; Wilcoxon–Mann–Whitney test, $p < 0.0001$). **E**, d4EGFP⁺ and d4EGFP⁻ IGCs demonstrate increased maximal action potential slope (d4EGFP⁺, $n = 26$; d4EGFP⁻, $n = 23$; Wilcoxon–Mann–Whitney test, $p < 0.05$). **F**, Sample traces for d4EGFP⁺ and d4EGFP⁻ IGCs for voltage-clamp ramp challenges. Traces displayed show responses to being held at -100 , -90 , -80 , -70 , -40 , and -20 mV. Calibration: 50 pA, 500 ms. **G**, I_h current ratio for d4EGFP⁺ and d4EGFP⁻ cells (d4EGFP⁺, $n = 26$; d4EGFP⁻, $n = 23$; Wilcoxon–Mann–Whitney test, $p = 0.24$). **H**, I_h subtracted currents following 10 μ M ZD7288 application for d4EGFP⁺ and d4EGFP⁻ IGCs (d4EGFP⁺ cells, $n = 10$; d4EGFP⁻ cells, $n = 10$; $n = 9$ mice; Wilcoxon–Mann–Whitney test, $p < 0.05$). * $p < 0.05$, **** $p < 0.0001$.

this cluster, indicating that increased IGC firing frequency was not associated with a systematic change in these other properties.

In assessing individual intrinsic properties, few differed significantly between d4EGFP⁺ and d4EGFP⁻ IGCs (Fig. 6C–H). The most noteworthy individual characteristic was an increase in spiking frequency in response to strong somatic depolarization in *Arc*-expressing IGCs (Wilcoxon–Mann–Whitney test, $p < 0.0001$; Fig.

6D). d4EGFP⁺ IGCs demonstrated an increase in the maximal slope of initial action potentials (Wilcoxon–Mann–Whitney test, $p < 0.05$; Fig. 6E), which was not a result of increased sodium current peak amplitudes (d4EGFP⁺, 2.33 ± 0.22 nA; d4EGFP⁻, 2.02 ± 0.14 nA; Wilcoxon–Mann–Whitney test, $p = 0.49$) or spike threshold (d4EGFP⁺, -23.5 ± 1.5 mV; d4EGFP⁻, -23.0 ± 1.3 mV; Wilcoxon–Mann–Whitney test, $p = 0.53$).

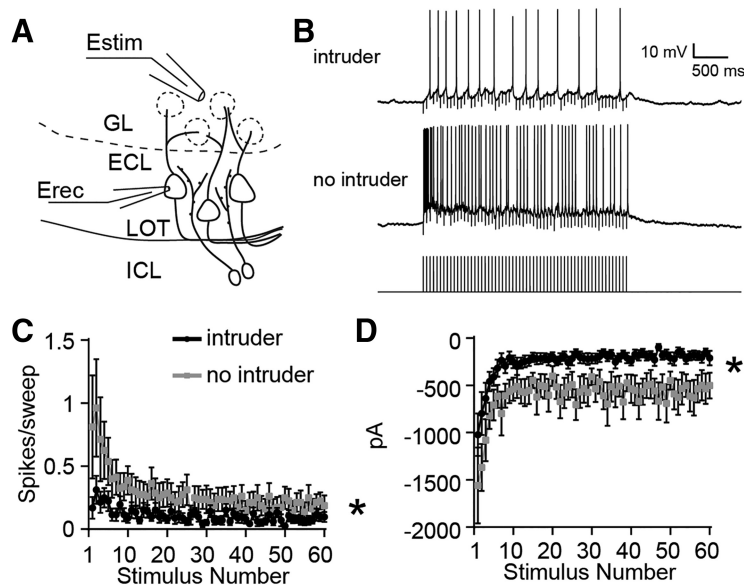


Figure 7. MCs show decreased excitation by glomerular stimulation following resident–intruder behavior. **A**, Diagram illustrating experimental setup. Estim, Theta glass-stimulating electrode; Erec, recording electrode. **B**, Sample MC responses to 3 s, 20 Hz glomerular layer (GL) stimulation from residents that interacted with an intruder and control residents (no intruder). **C**, Per-stimulus spike probability in response to each pulse of 3 s, 20 Hz stimulation while the cell was artificially brought to the subthreshold potential of -55 mV. Repeated-measures ANOVA, interaction between group and stimulus: $F_{(59,1298)} = 2.45$, $*p < 0.0001$. Behavior: $n = 14$ cells, $n = 4$ mice; no behavior: $n = 10$ cells, $n = 4$ mice. **D**, Peak current amplitude in response to 3 s, 20 Hz stimulation while the cell was held at -40 mV. Repeated-measures ANOVA, main effect of group: $F_{(1,22)} = 8.49$, $*p = 0.008$. Behavior: $n = 13$ cells, $n = 4$ mice; no behavior: $n = 9$ cells, $n = 4$ mice.

Arc-expressing IGCs also exhibited a slight decrease in I_H currents (Fig. 6G), which we confirmed by measuring the currents blocked by the hyperpolarization-activated cyclic nucleotide-gated (HCN) channel antagonist ZD7288 ($10 \mu\text{M}$; Wilcoxon–Mann–Whitney, $p < 0.05$; Fig. 6H). Because IGCs have high input resistance ($1.0 \pm 0.17 \text{ G}\Omega$; $n = 54$ IGCs), small-amplitude I_H currents resulted in prominent depolarization (“sag” potential) measured at the soma (d4EGFP⁺, 5.81 ± 0.62 mV; d4EGFP⁻, 8.37 ± 0.90 mV; Wilcoxon–Mann–Whitney test, $p = 0.11$). These basic I_H measurements were made after step hyperpolarization from a steady-state membrane potential near -70 mV, which may have obscured I_H conductances open near IGC resting potential. To measure the contributions of such conductances, we subtracted I_H sag potentials (reflecting conductances activated by the transition from approximately -70 to approximately -125 mV) from rebound depolarizations that occurred after the hyperpolarizing pulses (reflecting all I_H conductances). This analysis revealed a larger relative contribution of I_H conductances near resting potential in d4EGFP⁺ IGCs compared with d4EGFP⁻ IGCs, suggesting a slight shift in the voltage dependence of activation of HCN channels (d4EGFP⁺, 1.33 ± 0.57 mV; d4EGFP⁻, 0.23 ± 0.47 mV; Wilcoxon–Mann–Whitney test, $p = 0.059$). At face value, these I_H results were somewhat surprising. However, the modulation of I_H has been reported in *Arc*-dependent plasticity elsewhere in the brain (Shah, 2014). In many cases, the downregulation of I_H has been associated with increased neuronal excitability (Poolos et al., 2002; Brager and Johnston, 2007; Campanac et al., 2008; Yi et al., 2016).

It may be possible that *Arc* is required for the expression of experience-dependent increases in IGC excitability. To investigate this hypothesis, we used *Arc*-d2EGFP knock-in/knock-out animals (Wang et al., 2006). In *Arc*^{-/-} animals, d2EGFP is expressed in neurons that would normally express *Arc*. We repeated our intrinsic electrophysiological assay in acute slices taken from

Arc^{-/-} male residents. d2EGFP⁺ IGCs in *Arc*^{-/-} mice showed no differences in maximum spiking frequency (d2EGFP⁺, 34.34 ± 4.64 Hz, $n = 16$; d2EGFP⁻, 27.25 ± 4.38 Hz, $n = 12$; Wilcoxon–Mann–Whitney test, $p = 0.30$), I_H sag potential (d2EGFP⁺, 7.15 ± 0.71 mV, $n = 20$; d2EGFP⁻, 7.80 ± 1.31 mV, $n = 14$; Wilcoxon–Mann–Whitney test, $p = 0.45$), or I_H currents (I_H current ratio: d2EGFP⁺, 0.173 ± 0.025 , $n = 17$; d2EGFP⁻, 0.155 ± 0.029 , $n = 14$; Wilcoxon–Mann–Whitney test, $p = 0.80$) compared with d2EGFP⁻ IGCs from the same slices. These results suggest that *Arc* is required for the observed differences in excitability between *Arc*-expressing and nonexpressing IGCs following male–male social interaction.

MC responses to glomerular stimulation are suppressed following behavior

The increased excitability of *Arc*-expressing IGCs suggests that AOB MCs may experience stimulus-associated suppression following resident–intruder encounters. To test this hypothesis, we measured the responses of posterior AOB MCs to glomerular layer stimulation during the same 4–8 h postbehavior time window used in IGC recordings (Fig. 7). MCs in current clamp were depolarized via steady-state current injections to -55 mV (just below the action potential threshold) and exposed to 3 s, 20 Hz glomerular layer stimulation (Fig. 7B,C). We observed less evoked spiking activity in MCs in AOB slices taken from postbehavior resident males than no-intruder controls (repeated-measures ANOVA, interaction between group and stimulus: $F_{(59,1298)} = 2.45$, $p < 0.0001$; $n = 13$ cells, 4 mice for “intruder” group; $n = 9$ cells, 4 mice for “no intruder” group, Fig. 7B,C). Voltage-clamp experiments from these same cells held at -40 mV revealed suppressed net inward current during the stimulus trains (repeated-measures ANOVA, main effect of group: $F_{(1,22)} = 8.49$, $p = 0.008$; Fig. 7D). We observed no differences in net inward current when cells were held at -50 mV (nearer Cl^- reversal potential), indicating that the results at -40 mV reflect the influence of increased outward currents (repeated-measures ANOVA, no main effect of group: $F_{(1,22)} = 0.07$, $p = 0.80$). We did not observe increased MC intrinsic excitability postbehavior (MC maximum spiking frequency: postbehavior, 48.1 ± 2.5 Hz; control, 40.2 ± 2.1 Hz; Wilcoxon–Mann–Whitney test, $p = 0.13$) but did involve a small decrease in I_H currents (normalized I_H current ratio, 0.0342 ± 0.003 ; postbehavior I_H current ratio, 0.047 ± 0.005 ; Wilcoxon–Mann–Whitney test, $p = 0.035$). Importantly, these currents are much smaller than those observed in IGCs, which is consistent with recent observations in mitral cells (Gorin et al., 2016). These results confirm that male–male social chemosensory encounters are associated with subsequent MC suppression, which is consistent with an experience-dependent increase in IGC–MC inhibition.

Discussion

The AOB remains a mysterious sensory circuit. It is often considered to be a relay station for information about environmental

pheromones and kairomones, but there is ample evidence that the AOB also participates in experience-dependent plasticity (Brennan, 2009). Experience-dependent plasticity in the AOB has been studied almost exclusively in the female rodent AOB in the context of mating (Binns and Brennan, 2005; Brennan and Kendrick, 2006), but there are many other rodent behaviors that are strongly influenced by the AOS (Maruniak et al., 1986; Wysocki and Lepri, 1991; Stowers et al., 2002; Kimchi et al., 2007; Papes et al., 2010). The principal motivation for this work was a desire to learn more about experience-dependent AOB plasticity in the context of nonmating AOS-mediated behaviors.

We specifically chose to study the resident–intruder territorial aggression paradigm because it is a male-typical AOS-dependent behavior that induces robust IEG activation in the AOB (Maruniak et al., 1986; Wysocki and Lepri, 1991; Kumar et al., 1999; Stowers et al., 2002). *Arc* is upregulated in male and female rodent AOB IGCs following mating (Matsuoka et al., 2002a,b, 2003), suggesting that *Arc*-expressing IGCs may underlie the increased AOB inhibition observed in this context (Kaba and Keverne, 1988; Brennan et al., 1990). Our results show that *Arc* is selectively transcribed and translated in posterior AOB IGCs of male mice following male–male social chemosensory encounters (Figs. 1, 2). *Arc* upregulation in AOB IGCs after the resident–intruder assay requires AOS chemosensory signaling, indicating that this effect is not caused by brain processes (e.g., centrifugal neuromodulation) associated with other sensory systems (Figs. 2, 3).

The specific neurophysiological changes reported in *Arc*-expressing neurons in other brain regions vary widely and are often subtle (Wang et al., 2006; Ploski et al., 2008; Shepherd and Bear, 2011; Jakkamsetti et al., 2013). For example, *Arc*-deficient pyramidal neurons in visual cortex have an overall reduction in their orientation selectivity but retain experience-dependent refinement of this selectivity (Wang et al., 2006). In the context of novel environment exploration, *Arc*-expressing hippocampal pyramidal neurons do not show outright synaptic depression but instead are primed for mGluR-dependent LTD (Jakkamsetti et al., 2013). In the AOB, *Arc* upregulation is conspicuously absent in projecting MCs (Figs. 1, 2, 3). IGCs are physiologically and morphologically different from most of the principal cell types in which *Arc* has been studied. Specifically, IGCs are axonless and use reciprocal dendrodendritic synapses to communicate with MCs (Jia et al., 1999; Taniguchi and Kaba, 2001). IGCs also experience significant cellular turnover in adulthood and are replenished by adult-born neurons that migrate via the rostral migratory stream (Alvarez-Buylla and Garcia-Verdugo, 2002). The selective capacity of IGCs to upregulate *Arc* in response to social chemosensory experience suggests that these interneurons may be primary drivers of AOB experience-dependent plasticity.

There are several genetic tools for labeling and manipulating *Arc*-expressing cells in living mouse brain tissue (Wang et al., 2006; Grinevich et al., 2009; Guenther et al., 2013; Kawashima et al., 2014). We specifically chose *Arc-d4EGFP-BAC* reporter mice for our initial physiological experiments for two reasons. First, endogenous *Arc* expression in these mice is unperturbed. Second, the half-life of the d4EGFP reporter allowed us to visualize *Arc*-expressing cells in acute slices for several hours following behavior. *Arc-d2EGFP* knock-in/knock-out mice remain a helpful tool for exploring the *Arc* dependence of various forms of neuronal plasticity. However, experiments involving these mice use *Arc*-positive controls that are haploinsufficient for *Arc* and limit targeted physiology experiments to shorter time windows.

Previous studies of AOB IGC function used pharmacology to approximate the conditions present during salient social events

(Araneda and Firestein, 2006; Smith et al., 2009, 2015; Taniguchi et al., 2013). These studies revealed important features of IGC neuromodulation but did not investigate the cellular and synaptic changes that occur in IGCs activated by bona fide social behaviors. In *Arc-d4EGFP-BAC* mice, *Arc* expression in IGCs after resident–intruder encounters correlates with increased activation by sensory input (Fig. 4) and increased intrinsic excitability (Fig. 6). *Arc* expression has been associated with glutamate receptor trafficking in other contexts (Chowdhury et al., 2006; Shepherd et al., 2006; Waung et al., 2008). However, our data show that the increased network excitability of *Arc*-expressing IGCs is not related to an increase in EPSC frequency or amplitude, nor is there evidence of significant upregulation in the number of dendritic spines (Fig. 5). These results were somewhat surprising in light of previous work showing an increased size of the postsynaptic density on IGC dendrites in female mice 1 d after mating, suggesting increased excitatory drive on IGCs (Matsuoka et al., 2004). However, our experiments took place both in a different behavioral context and at an earlier time point, which could indicate that different mechanisms or time courses are present following male–male social encounters. The increased excitability seen in *Arc*-expressing cells in d4EGFP mice was not observed in *Arc*^{-/-} mice from the *Arc-d2EGFP* strain. This indicates that *Arc* participates in the intrinsic differences in AOB IGCs seen after resident–intruder encounters. Collectively, these data suggest that *Arc* expression in IGCs contributes to an increased intrinsic capacity to respond to sensory input.

IGCs do not receive direct excitation from VSN terminals in the AOB glomerular layer but are instead activated by glutamate release from MCs at reciprocal dendrodendritic synapses (Jia et al., 1999; Taniguchi and Kaba, 2001). MCs do not demonstrate experience-dependent increases in intrinsic excitability following resident–intruder encounters, suggesting that the increased IGC activation is specific to the IGC postsynaptic response. However, it is also possible that a change in presynaptic function in the MCs providing input to *Arc*-expressing IGCs contributes to this effect. To approach this question will require tools that label both *Arc*-expressing IGCs and their connected MCs in living tissue.

In our investigation of the intrinsic differences between *Arc*-expressing and nonexpressing cells, we used methods aimed at objectively classifying cells based on the expression of 26 specific characteristics. *Arc*-expressing and nonexpressing cells were segregated into clusters that differed in their capacity to sustain high-frequency spiking (Fig. 6). The increase in excitability was not a result of changes to voltage-gated sodium channel threshold, sodium current amplitudes, or macroscopic changes to voltage-gated potassium currents. However, this analysis did reveal a trend for *Arc*-expressing IGCs to possess smaller I_H currents, which we confirmed pharmacologically (Fig. 6). HCN channel expression has been noted in the AOB and in IGCs, but their specific role in AOB circuit function has not yet been determined (Hu et al., 2016). I_H is active at resting membrane potential and gives rise to rebound depolarization after relief from transient hyperpolarization (Robinson and Siegelbaum, 2003; Biel et al., 2009). At face value, the observed decrease in I_H is at odds with the increase in intrinsic excitability seen in *Arc*-expressing IGCs. However, several other studies have shown that plasticity-induced decreases in I_H are associated with increases in excitability (Poolos et al., 2002; Brager and Johnston, 2007; Campanac et al., 2008; Yi et al., 2016). One potential factor in the apparent excitatory influence of decreased I_H could be a shift in the voltage dependence of HCN channel activation, leading to an increased number of HCN channels that are open at rest. Overall, our results suggest

that experience-dependent plasticity modulates IGC I_h currents, perhaps selectively in postsynaptic/dendritic structures. (Lörincz et al., 2002; Yi et al., 2016).

We confirmed that posterior MC activity is suppressed in AOB slices from resident mice following the resident–intruder assay (Fig. 7). This observation supports the hypothesis that experience-dependent upregulation of IGC excitability in *Arc*-expressing cells contributes to MC suppression. The effects were relatively modest but were achieved despite lacking an experience-dependent marker to select for MCs that were active during the resident–intruder encounter. It is possible that this limitation precluded us from identifying other physiological changes in MCs that are induced following male–male social interaction.

The observed increases in IGC intrinsic excitability and MC suppression are present for at least 8 h following behavior. This suggests that MC activation upon re-exposure to the same male during this time window would be decreased, which may result in a change in male–male social interactions. In the context of the Bruce Effect, pheromonal learning is AOB dependent and can persist for many weeks (Brennan and Keverne, 1997). It may be the case that the AOS refines male–male social interactions over similar time courses, but the specific behavioral impacts and time courses of any effects remain to be elucidated. In sum, these data reveal that AOB experience-dependent plasticity involves *Arc* upregulation in IGCs, which results in increased MC inhibition through the upregulation of IGC intrinsic excitability. Furthermore, our data show that inhibitory plasticity in the AOB occurs across social contexts and is a general feature of the AOS.

References

- Alvarez-Buylla A, Garcia-Verdugo JM (2002) Neurogenesis in adult subventricular zone. *J Neurosci* 22:629–634. [Medline](#)
- Araneda RC, Firestein S (2006) Adrenergic enhancement of inhibitory transmission in the accessory olfactory bulb. *J Neurosci* 26:3292–3298. [CrossRef Medline](#)
- Belluscio L, Koentges G, Axel R, Dulac C (1999) A map of pheromone receptor activation in the mammalian brain. *Cell* 97:209–220. [CrossRef Medline](#)
- Biel M, Wahl-Schott C, Michalakis S, Zong X (2009) Hyperpolarization-activated cation channels: from genes to function. *Physiol Rev* 89:847–885. [CrossRef Medline](#)
- Binns KE, Brennan PA (2005) Changes in electrophysiological activity in the accessory olfactory bulb and medial amygdala associated with mate recognition in mice. *Eur J Neurosci* 21:2529–2537. [CrossRef Medline](#)
- Bolte S, Cordelières FP (2006) A guided tour into subcellular colocalization analysis in light microscopy. *J Microsc* 224:213–232. [CrossRef Medline](#)
- Brager DH, Johnston D (2007) Plasticity of intrinsic excitability during long-term depression is mediated through mGluR-dependent changes in I_h in hippocampal CA1 pyramidal neurons. *J Neurosci* 27:13926–13937. [CrossRef Medline](#)
- Brennan PA (2009) Outstanding issues surrounding vomeronasal mechanisms of pregnancy block and individual recognition in mice. *Behav Brain Res* 200:287–294. [CrossRef Medline](#)
- Brennan PA, Kendrick KM (2006) Mammalian social odours: attraction and individual recognition. *Philos Trans R Soc Lond B Biol Sci* 361:2061–2078. [CrossRef Medline](#)
- Brennan PA, Keverne EB (1997) Neural mechanisms of mammalian olfactory learning. *Prog Neurobiol* 51:457–481. [CrossRef Medline](#)
- Brennan PA, Kendrick KM, Keverne EB (1995) Neurotransmitter release in the accessory olfactory bulb during and after the formation of an olfactory memory in mice. *Neuroscience* 69:1075–1086. [CrossRef Medline](#)
- Brennan P, Kaba H, Keverne EB (1990) Olfactory recognition: a simple memory system. *Science* 250:1223–1226. [CrossRef Medline](#)
- Bruce HM (1959) An exteroceptive block to pregnancy in the mouse. *Nature* 184:105. [CrossRef Medline](#)
- Bruce HM, Parrott DM (1960) Role of olfactory sense in pregnancy block by strange males. *Science* 131:1526. [CrossRef Medline](#)
- Campana E, Daoudal G, Ankr N, Debanne D (2008) Downregulation of dendritic I_h in CA1 pyramidal neurons after LTP. *J Neurosci* 28:8635–8643. [CrossRef Medline](#)
- Chamero P, Marton TF, Logan DW, Flanagan K, Cruz JR, Saghatelian A, Cravatt BF, Stowers L (2007) Identification of protein pheromones that promote aggressive behaviour. *Nature* 450:899–902. [CrossRef Medline](#)
- Chowdhury S, Shepherd JD, Okuno H, Lyford G, Petralia RS, Plath N, Kuhl D, Huganir RL, Worley PF (2006) *Arc/Arg3.1* interacts with the endocytic machinery to regulate AMPA receptor trafficking. *Neuron* 52:445–459. [CrossRef Medline](#)
- Ferrero DM, Moeller LM, Osakada T, Horio N, Li Q, Roy DS, Cichy A, Spehr M, Touhara K, Liberles SD (2013) A juvenile mouse pheromone inhibits sexual behaviour through the vomeronasal system. *Nature* 502:368–371. [CrossRef Medline](#)
- Golowasch J, Thomas G, Taylor AL, Patel A, Pineda A, Khalil C, Nadim F (2009) Membrane capacitance measurements revisited: dependence of capacitance value on measurement method in nonisopotential neurons. *J Neurophysiol* 102:2161–2175. [CrossRef Medline](#)
- Gorin M, Tsitoura C, Kahan A, Watznauer K, Drose DR, Arts M, Mathar R, O'Connor S, Hanganu-Opatz IL, Ben-Shaul Y, Spehr M (2016) Interdependent conductances drive infraslow intrinsic rhythmogenesis in a subset of accessory olfactory bulb projection neurons. *J Neurosci* 36:3127–3144. [CrossRef Medline](#)
- Grinevich V, Kolleker A, Eliava M, Takada N, Takuma H, Fukazawa Y, Shigemoto R, Kuhl D, Waters J, Seeburg PH, Osten P (2009) Fluorescent *Arc/Arg3.1* indicator mice: a versatile tool to study brain activity changes in vitro and in vivo. *J Neurosci Methods* 184:25–36. [CrossRef Medline](#)
- Guenther CJ, Miyamichi K, Yang HH, Heller HC, Luo L (2013) Permanent genetic access to transiently active neurons via TRAP: targeted recombination in active populations. *Neuron* 78:773–784. [CrossRef Medline](#)
- Guthrie K, Rayhanabad J, Kuhl D, Gall C (2000) Odors regulate *Arc* expression in neuronal ensembles engaged in odor processing. *Neuroreport* 11:1809–1813. [CrossRef Medline](#)
- Hendrickson RC, Krauthamer S, Essenberg JM, Holy TE (2008) Inhibition shapes sex selectivity in the mouse accessory olfactory bulb. *J Neurosci* 28:12523–12534. [CrossRef Medline](#)
- Hu R, Ferguson KA, Whiteus CB, Meijer DH, Araneda RC (2016) Hyperpolarization-activated currents and subthreshold resonance in granule cells of the olfactory bulb. *Eneuro* 3:e0197–16.2016. [CrossRef Medline](#)
- Jakkamsetti V, Tsai NP, Gross C, Molinaro G, Collins KA, Nicoletti F, Wang KH, Osten P, Bassell GJ, Gibson JR, Huber KM (2013) Experience-induced *Arc/Arg3.1* primes CA1 pyramidal neurons for metabotropic glutamate receptor-dependent long-term synaptic depression. *Neuron* 80:72–79. [CrossRef Medline](#)
- Jia C, Chen WR, Shepherd GM (1999) Synaptic organization and neurotransmitters in the rat accessory olfactory bulb. *J Neurophysiol* 81:345–355. [Medline](#)
- Kaba H, Keverne EB (1988) The effect of microinfusions of drugs into the accessory olfactory bulb on the olfactory block to pregnancy. *Neuroscience* 25:1007–1011. [CrossRef Medline](#)
- Kawashima T, Kitamura K, Suzuki K, Nonaka M, Kamijo S, Takemoto-Kimura S, Kano M, Okuno H, Ohki K, Bito H (2013) Functional labeling of neurons and their projections using the synthetic activity-dependent promoter E-SARE. *Nat Methods* 10:889–895. [CrossRef Medline](#)
- Kawashima T, Okuno H, Bito H (2014) A new era for functional labeling of neurons: activity-dependent promoters have come of age. *Front Neural Circuits* 8:37. [CrossRef Medline](#)
- Kim Y, Venkataraju KU, Pradhan K, Mende C, Taranda J, Turaga SC, Arganda-Carreras I, Ng L, Hawrylycz MJ, Rockland KS, Seung HS, Osten P (2015) Mapping social behavior-induced brain activation at cellular resolution in the mouse. *Cell Rep* 10:292–305. [CrossRef Medline](#)
- Kimchi T, Xu J, Dulac C (2007) A functional circuit underlying male sexual behaviour in the female mouse brain. *Nature* 448:1009–1014. [CrossRef Medline](#)
- Kumar A, Dudley CA, Moss RL (1999) Functional dichotomy within the vomeronasal system: distinct zones of neuronal activity in the accessory olfactory bulb correlate with sex-specific behaviors. *J Neurosci* 19:RC32. [Medline](#)
- Larriva-Sahd J (2008) The accessory olfactory bulb in the adult rat: a cytological study of its cell types, neuropil, neuronal modules, and interactions with the main olfactory system. *J Comp Neurol* 510:309–350. [CrossRef Medline](#)
- Leinders-Zuffall T, Ishii T, Chamero P, Hendrix P, Oboti L, Schmid A, Kircher

- S, Pyrski M, Akiyoshi S, Khan M, Vaes E, Zufall F, Mombaerts P (2014) A family of nonclassical class I MHC genes contributes to ultrasensitive chemodetection by mouse vomeronasal sensory neurons. *J Neurosci* 34:5121–5133. [CrossRef Medline](#)
- Liberles SD (2014) Mammalian pheromones. *Annu Rev Physiol* 76:151–175. [CrossRef Medline](#)
- Longair MH, Baker DA, Armstrong JD (2011) Simple Neurite Tracer: open source software for reconstruction, visualization and analysis of neuronal processes. *Bioinformatics* 27:2453–2454. [CrossRef Medline](#)
- Lörincz A, Notomi T, Tamás G, Shigemoto R, Nusser Z (2002) Polarized and compartment-dependent distribution of HCN1 in pyramidal cell dendrites. *Nat Neurosci* 5:1185–1193. [CrossRef Medline](#)
- Madisen L, Zwingman TA, Sunkin SM, Oh SW, Zariwala HA, Gu H, Ng LL, Palmiter RD, Hawrylycz MJ, Jones AR, Lein ES, Zeng H (2010) A robust and high-throughput Cre reporting and characterization system for the whole mouse brain. *Nat Neurosci* 13:133–140. [CrossRef Medline](#)
- Maruniak JA, Wysocki CJ, Taylor JA (1986) Mediation of male mouse urine marking and aggression by the vomeronasal organ. *Physiol Behav* 37:655–657. [CrossRef Medline](#)
- Matsuoka M, Yamagata K, Sugiura H, Yoshida-Matsuoka J, Norita M, Ichikawa M (2002a) Expression and regulation of the immediate-early gene product Arc in the accessory olfactory bulb after mating in male rat. *Neuroscience* 111:251–258. [CrossRef Medline](#)
- Matsuoka M, Yoshida-Matsuoka J, Sugiura H, Yamagata K, Ichikawa M, Norita M (2002b) Mating behavior induces differential Arc expression in the main and accessory olfactory bulbs of adult rats. *Neurosci Lett* 335:111–114. [CrossRef Medline](#)
- Matsuoka M, Yoshida-Matsuoka J, Yamagata K, Sugiura H, Ichikawa M, Norita M (2003) Rapid induction of Arc is observed in the granule cell dendrites in the accessory olfactory bulb after mating. *Brain Res* 975:189–195. [CrossRef Medline](#)
- Matsuoka M, Kaba H, Moriya K, Yoshida-Matsuoka J, Costanzo RM, Norita M, Ichikawa M (2004) Remodeling of reciprocal synapses associated with persistence of long-term memory. *Eur J Neurosci* 19:1668–1672. [CrossRef Medline](#)
- Meeks JP, Jiang X, Mennerick S (2005) Action potential fidelity during normal and epileptiform activity in paired soma-axon recordings from rat hippocampus. *J Physiol* 566:425–441. [CrossRef Medline](#)
- Meeks JP, Arnson HA, Holy TE (2010) Representation and transformation of sensory information in the mouse accessory olfactory system. *Nat Neurosci* 13:723–730. [CrossRef Medline](#)
- Nunez-Parra A, Maurer RK, Krahe K, Smith RS, Araneda RC (2013) Disruption of centrifugal inhibition to olfactory bulb granule cells impairs olfactory discrimination. *Proc Natl Acad Sci U S A* 110:14777–14782. [CrossRef Medline](#)
- Oettl LL, Ravi N, Schneider M, Scheller MF, Schneider P, Mitre M, da Silva Gouveia M, Froemke RC, Chao MV, Young WS, Meyer-Lindenberg A, Grinevich V, Shusterman R, Kelsch W (2016) Oxytocin enhances social recognition by modulating cortical control of early olfactory processing. *Neuron* 90:609–621. [CrossRef Medline](#)
- Omura M, Mombaerts P (2014) Trpc2-expressing sensory neurons in the main olfactory epithelium of the mouse. *Cell Rep* 8:583–595. [CrossRef Medline](#)
- Pankevich DE, Baum MJ, Cherry JA (2004) Olfactory sex discrimination persists, whereas the preference for urinary odors from estrous females disappears in male mice after vomeronasal organ removal. *J Neurosci* 24:9451–9457. [CrossRef Medline](#)
- Papes F, Logan DW, Stowers L (2010) The vomeronasal organ mediates interspecies defensive behaviors through detection of protein pheromone homologs. *Cell* 141:692–703. [CrossRef Medline](#)
- Pérez-Gómez A, Bleyemehl K, Stein B, Pyrski M, Birnbaumer L, Munger SD, Leinders-Zufall T, Zufall F, Chamero P (2015) Innate predator odor aversion driven by parallel olfactory subsystems that converge in the ventromedial hypothalamus. *Curr Biol* 25:1340–1346. [CrossRef Medline](#)
- Plath N, Ohana O, Dammermann B, Errington ML, Schmitz D, Gross C, Mao X, Engelsberg A, Mahlke C, Welzl H, Kobalz U, Stawrakakis A, Fernandez E, Waltereit R, Bick-Sander A, Therstappen E, Cooke SF, Blanquet V, Würst W, Salmen B, et al (2006) Arc/Arg3.1 is essential for the consolidation of synaptic plasticity and memories. *Neuron* 52:437–444. [CrossRef Medline](#)
- Ploski JE, Pierre VJ, Smucny J, Park K, Monsey MS, Overeem KA, Schafe GE (2008) The activity-regulated cytoskeletal-associated protein (Arc/Arg3.1) is required for memory consolidation of pavlovian fear conditioning in the lateral amygdala. *J Neurosci* 28:12383–12395. [CrossRef Medline](#)
- Poolos NP, Migliore M, Johnston D (2002) Pharmacological upregulation of h-channels reduces the excitability of pyramidal neuron dendrites. *Nat Neurosci* 5:767–774. [CrossRef Medline](#)
- Robinson RB, Siegelbaum SA (2003) Hyperpolarization-activated cation currents: from molecules to physiological function. *Annu Rev Physiol* 65:453–480. [CrossRef Medline](#)
- Rodriguez I, Feinstein P, Mombaerts P (1999) Variable patterns of axonal projections of sensory neurons in the mouse vomeronasal system. *Cell* 97:199–208. [CrossRef Medline](#)
- Rothermel M, Carey RM, Puche A, Shipley MT, Wachowiak M (2014) Cholinergic inputs from Basal forebrain add an excitatory bias to odor coding in the olfactory bulb. *J Neurosci* 34:4654–4664. [CrossRef Medline](#)
- Scalia F, Winans SS (1975) The differential projections of the olfactory bulb and accessory olfactory bulb in mammals. *J Comp Neurol* 161:31–55. [CrossRef Medline](#)
- Shah MM (2014) Cortical HCN channels: function, trafficking and plasticity. *J Physiol* 592:2711–2719. [CrossRef Medline](#)
- Shakhawat AM, Gheidi A, Hou Q, Dhillon SK, Marrone DF, Harley CW, Yuan Q (2014) Visualizing the engram: learning stabilizes odor representations in the olfactory network. *J Neurosci* 34:15394–15401. [CrossRef Medline](#)
- Shepherd JD, Bear MF (2011) New views of Arc, a master regulator of synaptic plasticity. *Nat Neurosci* 14:279–284. [CrossRef Medline](#)
- Shepherd JD, Rumbaugh G, Wu J, Chowdhury S, Plath N, Kuhl D, Huganir RL, Worley PF (2006) Arc/Arg3.1 mediates homeostatic synaptic scaling of AMPA receptors. *Neuron* 52:475–484. [CrossRef Medline](#)
- Shipley MT, Halloran FJ, de la Torre J (1985) Surprisingly rich projection from locus coeruleus to the olfactory bulb in the rat. *Brain Res* 329:294–299. [CrossRef Medline](#)
- Smith RS, Weitz CJ, Araneda RC (2009) Excitatory actions of noradrenergic and metabotropic glutamate receptor activation in granule cells of the accessory olfactory bulb. *J Neurophysiol* 102:1103–1114. [CrossRef Medline](#)
- Smith RS, Hu R, DeSouza A, Eberly CL, Krahe K, Chan W, Araneda RC (2015) Differential muscarinic modulation in the olfactory bulb. *J Neurosci* 35:10773–10785. [CrossRef Medline](#)
- Stowers L, Holy TE, Meister M, Dulac C, Koentges G (2002) Loss of sex discrimination and male-male aggression in mice deficient for TRP2. *Science* 295:1493–1500. [CrossRef Medline](#)
- Taniguchi M, Kaba H (2001) Properties of reciprocal synapses in the mouse accessory olfactory bulb. *Neuroscience* 108:365–370. [CrossRef Medline](#)
- Taniguchi M, Yokoi M, Shinohara Y, Okutani F, Murata Y, Nakanishi S, Kaba H (2013) Regulation of synaptic currents by mGluR2 at reciprocal synapses in the mouse accessory olfactory bulb. *Eur J Neurosci* 37:351–358. [CrossRef Medline](#)
- Vazdarjanova A, Ramirez-Amaya V, Insel N, Plummer TK, Rosi S, Chowdhury S, Mikhael D, Worley PF, Guzowski JF, Barnes CA (2006) Spatial exploration induces ARC, a plasticity-related immediate-early gene, only in calcium/calmodulin-dependent protein kinase II-positive principal excitatory and inhibitory neurons of the rat forebrain. *J Comp Neurol* 498:317–329. [CrossRef Medline](#)
- Vousden DA, Epp J, Okuno H, Nieman BJ, van Eede M, Dazai J, Ragan T, Bito H, Frankland PW, Lerch JP, Henkelman RM (2015) Whole-brain mapping of behaviourally induced neural activation in mice. *Brain Struct Funct* 220:2043–2057. [CrossRef Medline](#)
- Wang KH, Majewska A, Schummers J, Farley B, Hu C, Sur M, Tonegawa S (2006) In vivo two-photon imaging reveals a role of arc in enhancing orientation specificity in visual cortex. *Cell* 126:389–402. [CrossRef Medline](#)
- Waung MW, Pfeiffer BE, Nosyreva ED, Ronesi JA, Huber KM (2008) Rapid translation of Arc/Arg3.1 selectively mediates mGluR-dependent LTD through persistent increases in AMPAR endocytosis rate. *Neuron* 59:84–97. [CrossRef Medline](#)
- Wysocki CJ, Lepri JJ (1991) Consequences of removing the vomeronasal organ. *J Steroid Biochem Mol Biol* 39:661–669. [CrossRef Medline](#)
- Yi F, Danko T, Botelho SC, Patzke C, Pak C, Wernig M, Südhof TC (2016) Autism-associated SHANK3 haploinsufficiency causes H channelopathy in human neurons. *Science* 352:aaf2669. [CrossRef Medline](#)